Hindawi
Geofluids
Volume 2021, Article ID 2435930, 18 pages
https://doi.org/10.1155/2021/2435930

Research Article

Nanopore Confinement Effect on the Phase Behavior of CO_2/Hydrocarbons in Tight Oil Reservoirs considering Capillary Pressure, Fluid-Wall Interaction, and Molecule Adsorption

Zhixue Zheng[1,2], **Yuan Di**[1,2] **and Yu-Shu Wu**[3]

[1]*College of Engineering, Peking University, Beijing 100871, China*
[2]*Institute of Energy, Peking University, Beijing 100871, China*
[3]*Department of Petroleum Engineering, Colorado School of Mines, Golden CO 80401, USA*

Correspondence should be addressed to Yuan Di; diyuan@mech.pku.edu.cn

Received 8 July 2021; Revised 25 July 2021; Accepted 9 August 2021; Published 21 August 2021

Academic Editor: Steffen Berg

The pore sizes in tight reservoirs are nanopores, where the phase behavior deviates significantly from that of bulk fluids in conventional reservoirs. The phase behavior for fluids in tight reservoirs is essential for a better understanding of the mechanics of fluid flow. A novel methodology is proposed to investigate the phase behavior of carbon dioxide (CO_2)/hydrocarbons systems considering nanopore confinement. The phase equilibrium calculation is modified by coupling the Peng-Robinson equation of state (PR-EOS) with capillary pressure, fluid-wall interaction, and molecule adsorption. The proposed model has been validated with CMG-Winprop and experimental results with bulk and confined fluids. Subsequently, one case study for the Bakken tight oil reservoir was performed, and the results show that the reduction in the nanopore size causes noticeable difference in the phase envelope and the bubble point pressure is depressed due to nanopore confinement, which is conductive to enhance oil recovery with a higher possibility of achieving miscibility in miscible gas injection. As the pore size decreases, the interfacial tension (IFT) decreases whereas the capillary pressure increases obviously. Finally, the recovery mechanisms for CO_2 injection are investigated in terms of minimum miscibility pressure (MMP), solution gas-oil ratio, oil volume expansion, viscosity reduction, extraction of lighter hydrocarbons, and molecular diffusion. Results indicate that nanopore confinement effect contributes to decrease MMP, which suppresses to 650 psi (65.9% smaller) as the pore size decreases to 2 nm, resulting in the suppression of the resistance of fluid transport. With the nanopore confinement effect, the CO_2 solution gas-oil ratio and the oil formation volume factor of the oil increase with the decrease of pore size. In turn, the oil viscosity reduces as the pore size decreases. It indicates that considering the nanopore confinement effect, the amount of gas dissolved into crude oil increases, which will lead to the increase of the oil volume expansion and the decrease of the viscosity of crude oil. Besides, considering nanopore confinement effect seems to have a slightly reduced effect on extraction of lighter hydrocarbons. On the contrary, it causes an increase in the CO_2 diffusion coefficient for liquid phase. Generally, the nanopore confinement appears to have a positive effect on the recovery mechanisms for CO_2 injection in tight oil reservoirs. The developed novel model could provide a better understanding of confinement effect on the phase behavior of nanoscale porous media in tight reservoirs. The findings of this study can also help for better understanding of a flow mechanism of tight oil reservoirs especially in the case of CO_2 injection for enhancing oil recovery.

1. Introduction

According to the predictions, global energy demand is projected to grow by about a third by 2040, particularly in India, China, and across Asia [1]. Tight oil reservoirs have been increasingly concerned due to its abundant reserves, huge development, and utilization potential. As illustrated in EIA's crude oil production forecast graph from 2020 annual report, tight oil in the United States is predicted to increase the total amount of crude oil production by 160% from 2010 to 2050. Tight oil production will more than double from 2015 to 2040 as shown in Figure 1 [2]. To meet oil

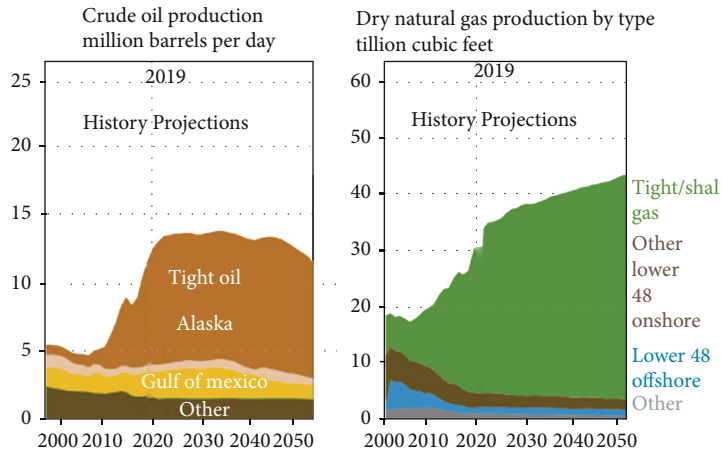

Figure 1: Historical and projected sources of crude oil and natural gas in the US (EIA, 2020).

demand, substantial ongoing investment in tight oil reservoir development will be required.

Despite horizontal drilling and multistage hydraulic fracturing technologies achieving tremendous success for economic development of tight oil reservoirs, the oil industry still faces challenges such as low oil recovery and rapidly declining production rate due to unknown fluid phase behavior and recovery mechanisms in tight oil reservoirs accurately [3–6]. Therefore, understanding the phase behavior for fluids in nanopores is essential for a better developing tight oil reservoirs and predicting well performance.

The pore sizes in tight reservoirs are nanopores, where the phase behavior deviates significantly from that of bulk fluids in conventional reservoirs [7–9]. Wang et al. [10] conducted nanofluidic device experiments with pure alkane and showed that the vaporization of the liquid phase in nanochannels is obviously suppressed compared to that in microchannels. Nojabaei et al. [11] found that the PVT properties of crude oil were significantly different under the two conditions comparing the PVT properties of crude oil in a PVT cylinder with those in nanoscale porous media. Luo et al. [12, 13] studied nanopore confinement effect using differential scanning calorimetry (DSC) and found that the bubble point alteration is significant when the pore size under 4.1 nm. Pinho et al. [14] introduced a novel technique to conduct a microfluidic multicomponent phase behavior and showed that multicomponent P-T diagrams are altered under nanopore confinement effect. Other experimental techniques including temperature-programmed desorption (TPD) [15], neutron diffraction [16], volumetric measurement [17], X-ray diffraction [18], scanning electron microscope (SEM) [19], and micro-CT scanning [20] also have found similar phenomena in nanopores. All these experiments showed that nanoscale interaction had a remarkable effect on the gas-liquid equilibrium of hydrocarbon components, but the results were influenced by experimental materials, and there were few experimental studies on the phase behavior in nanopores with a radius smaller than 50 nm was present in the literature due to the unconventional characteristics of tight oil reservoirs and the limitations of laboratory equipment. Molecular simulation is also widely used to investigate the fluid phase behavior under nanopore confinement. Wang et al. [21] presented Monte Carlo simulation (MC) to investigate the adsorption behavior of pentane, heptane, and their mixtures in slit-nanopores and found that multiple adsorption layers properties depend on pore size and fluid compositions. Jin and Firoozabadi [22] analyzed the effect of pore size distribution by gauge-GCMC simulation and revealed that fluids in tiny pores condense before that in large pores, and the shift of the phase diagram would increase with the proportion of small pores. Despite these simulation studies providing details of the behavior of confined fluids, it is not applicable to employ the molecular simulation method to analyze the nanopore confinement effect on the phase behavior at an engineering scale due to their high computation costs. Therefore, researchers have focused on developing thermodynamics models to characterize the fluid phase behavior of confined tight oil reservoirs.

The equation of state (EOS) is one of the most used approaches in thermodynamics models, and it has accomplished a huge success in modeling bulk phase behavior. Recently, experimental and theoretical studies have shown the existence of capillary pressure effect in nanopores. In an effort to consider the nanopore confinement effect on the phase behavior in tight oil reservoirs, Zhang et al. [23] modified flash calculation with capillary pressure and performed the studies of the phase behavior of CO_2/hydrocarbons systems in Bakken formations, and the results indicated that the capillary pressure effect cannot be neglected in nanopores. MMP of CO_2 injection decreases with the capillary pressure effect, resulting in the suppression of the resistance of fluid transport. Li and Sheng [24] performed the phase equilibrium of Wolfcamp shale reservoir by coupling Peng-Robinson equation of state (PR-EOS) with capillary pressure and shifted critical properties, and results presented that nanopore confinement narrowed the two-phase region and decreased the interfacial tension. The confined space in tight oil reservoirs causes the molecular radius to be comparable to the pore size, and the interaction between the fluid molecular and pore wall strengthens to a point that cannot be ignored. Yang et al. [25] recently

revealed the size effect of the solid-liquid interface energy and found that the mechanical action of the solid-liquid interface plays an important role in capillary condensation under nanometer or subnanometer scale, rather than the gas-liquid interface, which is generally believed to play a dominant role. In order to consider the influence of the interaction between the fluid and pore wall on the phase equilibrium, Travalloni et al. [26] proposed a modified PR-EOS considering both molecule–molecule and molecule-wall interaction and claimed that the molecule-wall interaction cannot be negligible. Yang et al. [27] extended PR-EOS by introducing a new term representing the molecule-wall interaction and showed that the molecule-wall interaction causes a significant alteration of the two-phase region. Adsorption has been an important factor in studying the fluid phase behavior under nanopore confinement. Dong et al. [28] coupled the multicomponent potential theory of adsorption with PR-EOS to investigate the fluid phase behavior of pure hydrocarbons and their mixtures in organic slit-like and cylindrical nanopores and showed that adsorption played an important role in the fluid phase behavior. Cui et al. [29] improved PR-EOS by reducing mole number of fluids caused by adsorption. Sandoval et al. [30] explored the adsorption effect on the fluid phase behavior in nanopores and incorporated the adsorption film thickness into the calculation of the effective capillary radius. Song et al. [31] introduced a novel method for describing fluid adsorption in nanopores by modifying the molar volume term in PR-EOS and showed that adsorption induced critical shifts of confined fluids in nanopores.

As mentioned above, nanopore confinement effects including capillary pressure, fluid-wall interaction, and molecule adsorption cannot be ignored in porous media with pore diameters less than 50 nm and greater than 2 nm [32–34]. Although numerous models have been proposed to explore the phase behavior in nanopores, they focused on one or both aspects of nanoscale confinement [23–31], and there still lack an accurate model that takes into account capillary pressure, fluid-wall interaction, and adsorption effect simultaneously. Additionally, despite methods being there to investigate nanopore confinement effect, only a few of them have studies the influence of nanopore confinement effect on CO_2 injection recovery mechanisms in tight oil reservoirs. Motivated by these points, a modified PR-EOS model is established to study the fluid phase behavior and recovery mechanisms in tight oil reservoirs for CO_2 injection.

The rest of the paper is organized as follows. In Section 2, the methodology section illustrates the procedures of model development by coupling fluid-wall interaction and adsorption effect in the EOS and capillary pressure in the flash calculation. Subsequently, the proposed model is validated with CMG-Winprop and experimental results with bulk and confined fluids, and then, we performed to analyze one case study from the Bakken tight oil reservoir at various pore sizes in Section 3. In Section 4, based on the investigation of the phase behavior of tight oil with CO_2 injection under different scenarios, the recovery mechanisms affected by minimum miscible pressure (MMP), solution gas-oil ratio, oil volume expansion, viscosity reduction, extraction of lighter hydrocarbons, and molecular diffusion are studied with respect to the confinement effect. At the end, summary and conclusions are provided in Section 5 to give some suggestions. The developed novel model provides a better understanding of confinement effect on the phase behavior in tight reservoirs and even nanoscale porous media. The findings of this study can also help for better understanding of the flow mechanism of tight oil reservoirs especially in the case of CO_2 injection for enhancing oil recovery.

2. Materials and Methods

The fluid phase behavior in tight oil reservoirs is governed by the interactions of fluid-fluid and fluid-wall interactions within the confining geometry [11]. In the pore networks, fluid molecules are usually adsorbed onto the pore wall [35–37]. At large pore sizes, the number of molecules adsorbed is negligible compared to the volume of the liquid. When the pore size decreases further (<10 nm), the interaction between molecules and pore walls of porous media is significant [32]. Adsorption will be significant and greatly reduces the number of fluid molecules in the free state which then will affect the molecular molar volume. In the nanopores, the larger capillary pressure, van der Waals forces, fluid-wall interaction, and adsorption effect lead to the deviation of physical properties in the bulk fluid.

In this section, the methodology is introduced to describe the nanopore confinement effect on the phase behavior, and the PR-EOS and Rachford-Rice flash calculation are modified considering capillary pressure, fluid-wall interaction, and adsorption effect.

2.1. Fluid-Wall Interaction. The original PR-EOS consists of a repulsion pressure P_R and an attraction pressure P_A as follows [38]:

$$P = P_R + P_A = \frac{RT}{V_m - b} - \frac{a}{V_m(V_m + b) + b(V_m - b)}, \quad (1)$$

$$P_R = \frac{RT}{V_m - b}, \quad (2)$$

$$P_A = -\frac{a}{V_m(V_m + b) + b(V_m - b)}, \quad (3)$$

where P is the system pressure, R is the gas constant, T is the system temperature, V_m is the molar volume, a represents "attraction" parameter, and b is the van der Waals co-volume, which represent "repulsion" parameter.

In nanopores, in order to consider fluid-wall interaction effect, we introduce a molecule-wall interaction pressure term P_{FW} which plays a role of diminishing the attractive component [25] into Equation (1) as follows:

$$P = \frac{RT}{V_m - b} - \frac{a}{V_m(V_m + b) + b(V_m - b)} + \frac{c}{V_m(V_m + b) + b(V_m - b)},$$
$$P_{\mathrm{FW}} = \frac{c}{V_m(V_m + b) + b(V_m - b)}, \tag{4}$$

where c is the fluid-wall interaction effect coefficient.

2.2. Adsorption Effect. There are many models describing the adsorption effect, such as ideal adsorbed solution theory, multicomponent potential theory of adsorption, and Langmuir isothermal adsorption model [39–41]. For the sake of incorporating the adsorption effect on nanopore confinement conveniently, in this paper, the fluid molecules adsorbed in the organic matters and pore walls are assumed stationary, and adsorption leads to the reduction number of movable fluid molecules, which in turn increases the effective mole volume of fluid molecules in the bulk phase [29]. An adsorption effect coefficient α is introduced into Equation (1) as follows:

$$P = \frac{RT}{\alpha V_m - b} - \frac{a}{\alpha V_m(\alpha V_m + b) + b(\alpha V_m - b)}. \tag{5}$$

2.3. The Modified PR-EOS. The original PR-EOS could be modified by two parameters representing separately fluid-wall interaction and adsorption effect. Then, the PR-EOS is modified as follows:

$$P = \frac{RT}{\alpha V_m - b} - \frac{a - c}{\alpha V_m(\alpha V_m + b) + b(\alpha V_m - b)}. \tag{6}$$

From Equation (6), it can be seen that when $\alpha = 1$ and $c = 0$, that is to say, fluid-wall interaction and adsorption effect are not taken into account, the modified PR-EOS can be reduced to original PR-EOS.

For the PR-EOS, the isotherm merely has a horizontal tangent and inflection point at the critical point in the typical pressure-volume diagram [42]. This can be expressed mathematically that the first and second derivatives of pressure with respect to volume at a constant temperature are equal to 0.

$$\left(\frac{\partial P}{\partial V}\right)_{T=T_c} = \left(\frac{\partial^2 P}{\partial V^2}\right)_{T=T_c} = 0, \tag{7}$$

where T_c represents the critical temperature.

Imposing Equation (7) on Equation (6) and parameters $a - c$ and b yields could be expressed by

$$a - c = 0.45724\frac{R^2 {T_C}^2}{P_c}, \tag{8}$$

$$b = 0.07780\frac{RT_c}{\alpha P_c}. \tag{9}$$

The details of "$a - c$ " and "b" calculations are specified in the Appendix. From Equations (6)–(9), the expressions of critical pressure and critical temperature can be obtained as follows:

$$P_{\mathrm{CC}} = 0.01324\frac{a - c}{\alpha^2 b^2},$$
$$T_{\mathrm{CC}} = 0.17015\frac{a - c}{\alpha b R}, \tag{10}$$

where P_{CC} and T_{CC} are the critical pressure and critical temperature determined by the modified PR-EOS.

The dimensionless shifts of critical pressure ΔP and critical temperature ΔT are defined as follows:

$$\Delta P = \frac{P_c - P_{\mathrm{cc}}}{P_c} = \frac{a\alpha^2 - a + c}{a\alpha^2}, \tag{11}$$

$$\Delta T = \frac{T_c - T_{\mathrm{cc}}}{T_c} = \frac{a\alpha - a + c}{a\alpha}. \tag{12}$$

2.4. Correlation for Critical Pressure and Critical Temperature. Equations (11) and (12) exhibit that fluid-wall interaction and adsorption effect influence the critical pressure and critical temperature in nanopores. It has been reported that the pore size r_p and collision diameter σ_{LJ} (Lennard-Jones molecular size parameter) are the important factors on shifts of critical pressure and critical temperature [27, 31]. The confined fluid critical pressure shift and critical temperature shift for different components (CO_2, CH_4, C_2H_4, C_2H_6, C_4H_{10}, C_8H_{18}, and $C_{10}H_{22}$) are collected from references [43–51]. Then, the correlations between the shifts of critical properties and the dimensionless pore size (r_p/σ_{LJ}) can be obtained and demonstrated in Figures 2(a) and 2(b).

As described in Figures 2(a) and 2(b), the correlations of shifts of critical pressure and critical temperature with dimensionless pore size are

$$\Delta P = 0.9793\left(\frac{r_p}{\sigma_{LJ}}\right)^{-0.6366},$$
$$\Delta T = 0.7597\left(\frac{r_p}{\sigma_{LJ}}\right)^{-0.7708}, \tag{13}$$

where r_p is the radius of pore throat and σ_{LJ} is the Lennard-Jones molecular size parameter.

From Equations (11) and (12), both fluid-wall interaction effect coefficient α and adsorption effect coefficient c can be calculated by shifts of critical pressure and temperature.

$$\alpha = \frac{1-\Delta T}{1-\Delta P} = \frac{1 - 0.7597\left(r_p/\sigma_{LJ}\right)^{-0.7708}}{1 - 0.9793\left(r_p/\sigma_{LJ}\right)^{-0.6366}},$$
$$c = (1 - \alpha(1-\Delta T))a = \left(1 - \frac{\left(1 - 0.7597\left(r_p/\sigma_{LJ}\right)^{-0.7708}\right)^2}{1 - 0.9793\left(r_p/\sigma_{LJ}\right)^{-0.6366}}\right)a. \tag{14}$$

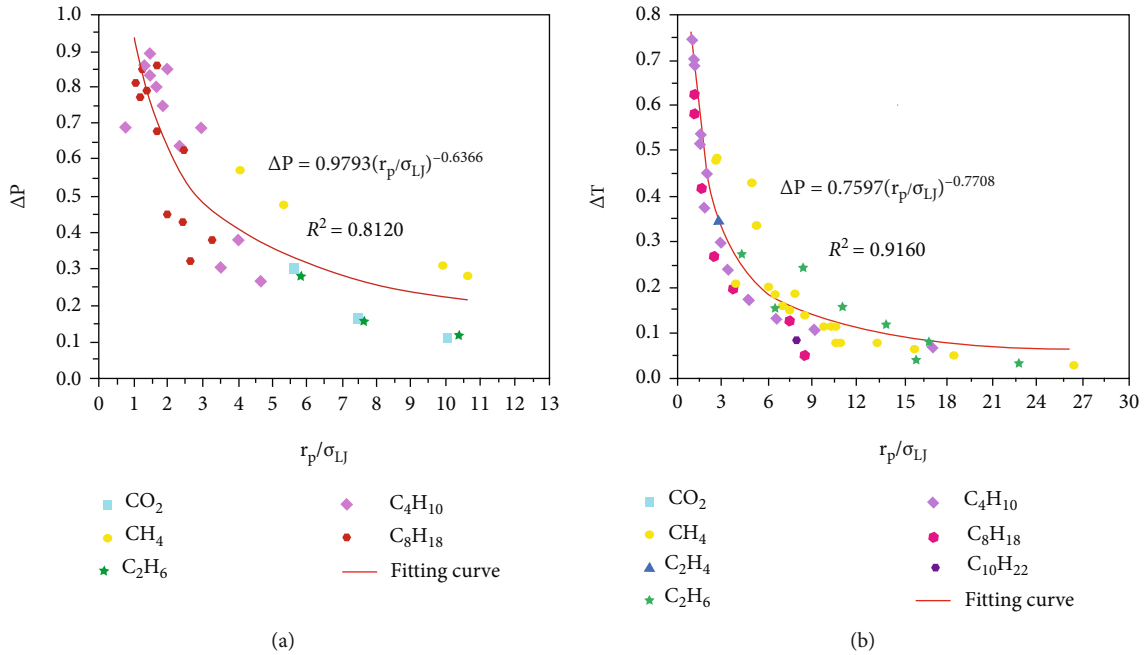

Figure 2: (a) Correlation of shift of critical pressure and (b) correlation of shift of critical temperature with the dimensionless pore size.

2.5. Phase Equilibrium Calculation considering Capillary Pressure, Fluid-Wall Interaction, and Molecule Adsorption. According to the thermodynamic theory, for a system containing N_c components, the thermodynamic condition for the phase equilibrium state is that when the temperature and pressure of each phase are equal, the chemical potential or fugacity of each component is equal.

$$\begin{aligned} f_i^L(T, P_L, x_i) &= f_i^V(T, P_V, y_i) i = 1, 2, \cdots, N_c, \\ f_i^L &= x_i \varphi_i^L P_L, \\ f_i^V &= y_i \varphi_i^V P_V, \end{aligned} \tag{15}$$

where f_i^L and f_i^V are fugacity of component i in the liquid and vapor phases, respectively. x_i and y_i are the mole fraction of component i in the liquid and vapor phases, respectively. P_L and P_V are the liquid and vapor pressures, respectively. φ_i^L and φ_i^V are the fugacity coefficient of component i in the liquid and vapor phases. N_c is the number of components.

According to the mass balance equation, Rachford and Rice [52] proposed an isothermal flash calculation method to determine the equilibrium phase composition and mole fraction of the component in the liquid and gas phases. The mass balance equation and Rachford-Rice equation are presented in

$$\sum_{i=1}^{N_c} x_i = \sum_{i=1}^{N_c} y_i = 1 \; i = 1, 2, \cdots, N_c, \tag{16}$$

$$z_i = (1 - n_V) x_i + n_V y_i, \tag{17}$$

$$\sum_{i=1}^{N_c} \frac{(K_i - 1) z_i}{1 + n_V (K_i - 1)} = 0 \; i = 1, 2, \cdots, N_c, \tag{18}$$

where z_i is the overall mole fraction of component i. n_V is overall number of moles in vapor phase. K_i is phase equilibrium ratio of component i.

The difference between liquid pressure and vapor pressure is defined as capillary pressure P_{cap}, which is calculated by the Young-Laplace equation [53]:

$$P_{cap} = P_V - P_L = \frac{2\sigma \cos\theta}{r_p}, \tag{19}$$

where θ is the contact angle. r_p is the radius of pore throat. σ is the interfacial tension which can be calculated by Macleod-Sugden correlation [54] as follows:

$$\sigma = \left[\sum_{i=1}^{N_c} \left(\rho_L x_i [P]_i - \rho_V y_i [P]_i \right) \right]^4, \tag{20}$$

where ρ_L and ρ_V are the densities of liquid phase and vapor phase, respectively. $[P]_i$ is the parachor of component i in the liquid or vapor phase.

The formula of the compressibility factor in nanopores is presented as follows:

$$Z = \frac{\alpha P V_m}{RT}, \tag{21}$$

where Z is the compressibility factor.

Hence, rearranging Equation (6) into the compressibility factor form rewrites

$$Z^3 - (1 - B) Z^2 + \left(A - 3B^2 - 2B \right) Z - \left(AB - B^2 - B^3 \right) = 0, \tag{22}$$

where

$$A = \frac{(a-c)P}{(RT)^2},$$
$$B = \frac{bP}{\alpha RT}. \tag{23}$$

Since the pressures of the liquid and vapor phases are not equal, Equation (21) can be separately rewritten for liquid phase with the following:

$$Z_L{}^3 - (1-B_L)Z_L{}^2 + \left(A_L - 3B_L{}^2 - 2B_L\right)Z_L - \left(A_L B_L - B_L{}^2 - B_L{}^3\right) = 0, \tag{24}$$

where Z_L is the compressibility factor of the liquid phase.

Similarly, for vapor phase is as follows:

$$Z_V{}^3 - (1-B_V)Z_V{}^2 + \left(A_V - 3B_V{}^2 - 2B_V\right)Z_V - \left(A_V B_V - B_V{}^2 - B_V{}^3\right) = 0, \tag{25}$$

where Z_V is the compressibility factor of the vapor phase.

The fugacity coefficient for the liquid and vapor phases are defined by the following expressions:

$$\ln \varphi_{\mathrm{i}}^{\mathrm{L}} = -\ln\left[Z_L - B_L\right] + \frac{b_{iL}}{b_L}(Z_L - 1) + \frac{A_L}{2\sqrt{2}B_L} \cdot \left[\frac{2\sum_{i=1}^{N_c} x_{jL}\left(1-k_{ij}\right)\sqrt{a_{iL}a_{jL}}}{a_L} - \frac{b_{iL}}{b_L}\right] \ln\left[\frac{Z_L + B_L\left(1+\sqrt{2}\right)}{Z_L + B_L\left(1-\sqrt{2}\right)}\right],$$

$$\ln \varphi_{\mathrm{i}}^{\mathrm{V}} = -\ln\left[Z_V - B_V\right] + \frac{b_{iV}}{b_V}(Z_V - 1) + \frac{A_V}{2\sqrt{2}B_V} \cdot \left[\frac{2\sum_{i=1}^{N_c} x_{jV}\left(1-k_{ij}\right)\sqrt{a_{iV}a_{jV}}}{a_V} - \frac{b_{iV}}{b_V}\right] \ln\left[\frac{Z_V + B_V\left(1+\sqrt{2}\right)}{Z_V + B_V\left(1-\sqrt{2}\right)}\right]. \tag{26}$$

Hence, the liquid-vapor phase equilibrium accounting for the capillary pressure effect can be obtained using the aforementioned equations. Successive substitution and Newton-Raphson method are applied for solving nonlinear equations. Figure 3 demonstrates the flow chart for the phase equilibrium calculation with the nanopore confinement effect considering capillary pressure, fluid-wall interaction, and molecule adsorption.

3. Model Validation and Analysis

3.1. Model Validation. To validate the accuracy of modified model considering capillary pressure, fluid-wall interaction, and molecule adsorption effect, in this section, the developed model results are compared with CMG-Winprop results and experimental results. The phase equilibrium ratio (K-value) of fluid components in Tahe Oilfield in China at $T = 124.4°\mathrm{C}$ and $P = 20.78\,\mathrm{MPa}$ is first calculated. The fluid type in Tahe Oilfield is bulk fluids.

The predicted results and CMG-Winprop results are summarized in Table 1. Furthermore, we calculate the phase equilibrium ratio (K-value) of fluid components at $T = 344.8$ K and $P = 61.8\,\mathrm{psi}$. The data from experimental studies are reported in the literature [10], and the fluid type is confined fluids. The predicted results and experimental results are summarized in Table 2. The compared analysis indicates a good agreement between the developed model data with CMG-Winprop and experimental results. The average deviation between the predicted K-value and CMG-Winprop results is 2.71%, indicating that the modified model proposed in this study can effectively predict the phase behavior of fluids in bulk. The average deviation between the predicted K-value and experimental results is 1.02%. Compared with the model only considering capillary pressure whose average deviation is 2.78%, the error is more acceptable.

3.2. Nanopore Confinement Effect on Phase Behavior of Fluids in Bakken Tight Oil Reservoir. The Bakken tight oil reservoir is one of the largest tight oil resources in the world, with total daily production exceeding $19 \times 104\,\mathrm{t}$. In this study, we investigate the nanopore confinement effect on the phase behavior of a typical fluid in Bakken tight oil reservoirs. The composition and physical property parameters of crude oil are taken from Zhang and Yu et al. [32, 55], which are shown in Tables 3 and 4, respectively.

3.2.1. Phase Envelope. The modified model is used to determine the phase envelope of the Bakken tight oil reservoir for the pore radius ranging from 5 nm to 50 nm. Figure 4 conducts the sensitivity analyses of pore size on the phase envelope by separately considering capillary pressure, fluid-wall interaction, and adsorption effect. As shown in Figure 4(a) where only capillary pressure is considered, the bubble point curve is lowered as the pore size decreases. After considering capillary pressure, the bubble point pressure is obviously suppressed when the pore size is less than 50 nm. The significant changes caused by the capillary pressure effect on bubble point pressures can reach as high as 630 psi when the pore size reduces to 5 nm. As the system goes above the bubble point pressure, the fluids in the Bakken tight oil reservoir may remain in the single-phase region. When the pressure is lower than the bubble point pressure, the amount of light or medial hydrocarbons tend to be evaporated to the form of gas bubble. Hence, the reduction in the bubble point pressure delays the process of vapor extracts out of the liquid and indicates that the fluids may remain in the liquid phase much longer. Therefore, considering capillary pressure has a positive influence on the tight oil

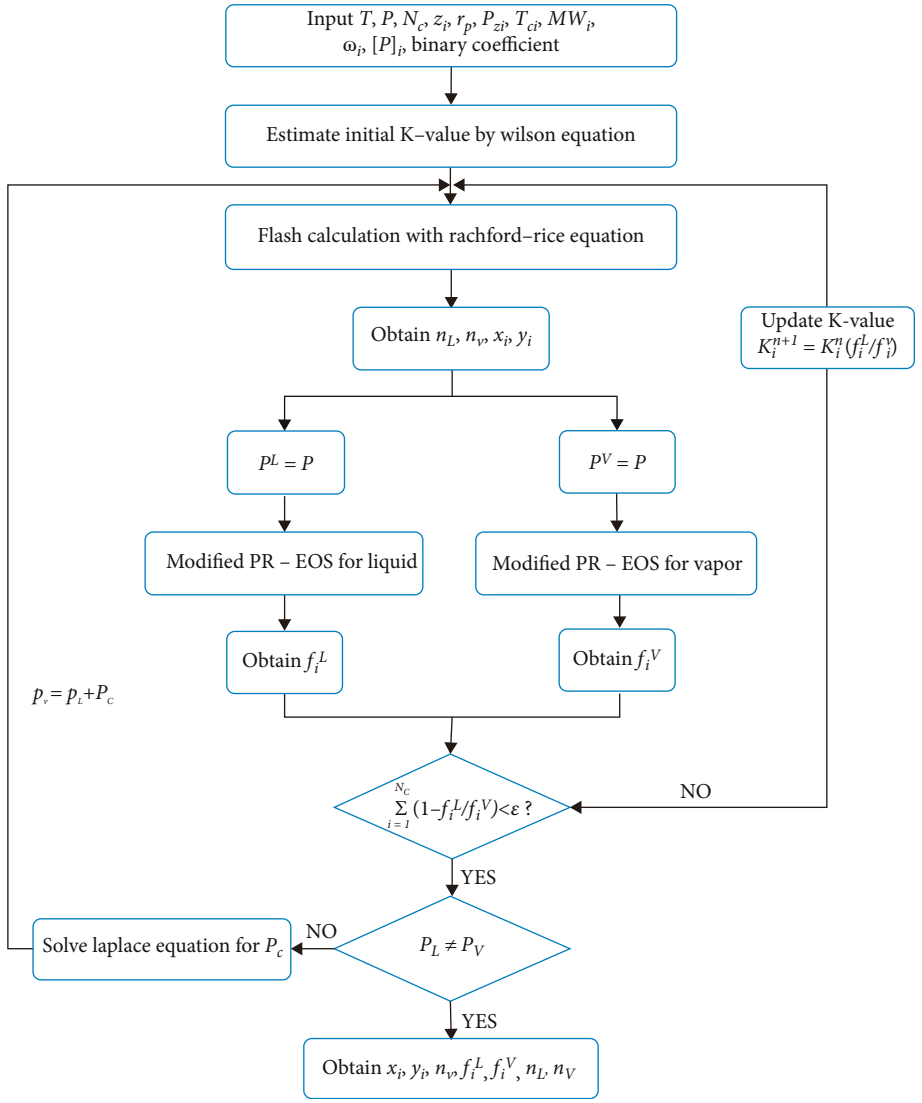

Figure 3: Flow char for phase equilibrium calculation with modified PR-EOS.

Table 1: Comparison of phase equilibrium ratio between predicted results and CMG-Winprop results.

Fluid types	Components	Molar fraction (%)	CMG-Winprop results	Simulation results	Relative deviation (%)
Bulk fluids	C_1	43.96	2.3186	2.3798	2.64
	C_2-C_4	21.03	1.0071	0.9943	1.27
	C_5-C_7	6.81	0.3447	0.3337	2.94
	C_8-C_9	7.59	0.1897	0.1823	3.90
	C_{10+}	18.71	0.0068	0.0070	3.13
	CO_2	1.90	1.6850	1.7255	2.40

Table 2: Comparison of phase equilibrium ratio between predicted results and experimental or simulation results.

Fluid types	Components	Molar fraction (%)	Experimental data	Simulation results with P_c	Relative deviation (%)	Simulation results this paper	Relative deviation (%)
Confined fluids	i-C_4	61.89	2.652	2.816	6.18	2.594	2.19
	n-C_4	18.11	1.885	1.904	1.01	1.894	0.48
	C_8	20.00	0.0524	0.053	1.15	0.0522	0.38

Table 3: The composition and physical property parameters of crude oil for the Bakken formation.

Components	T_{ci} (K)	P_{ci} (bar)	V_c (L/mol)	MW_i (g/mol)	ω_i	Parachor	z_i (%)
C_1	190.60	45.40	0.0990	16.04	0.0080	77.0	25.06
C_2-C_4	363.30	42.54	0.1970	42.82	0.1432	145.2	22.00
C_5-C_7	511.56	33.76	0.3338	83.74	0.2474	250.0	20.00
C_8-C_9	579.34	30.91	0.4062	105.91	0.2861	306.0	13.00
C_{10+}	788.74	21.58	0.9208	200.00	0.6869	686.3	19.94

Table 4: Binary interaction parameters for oil components.

Components	C_1	C_2-C_4	C_5-C_7	C_8-C_9	C_{10+}
C_1	0	0.0078	0.0242	0.0324	0.0779
C_2-C_4	0.0078	0	0.0046	0.0087	0.0384
C_5-C_7	0.0242	0.0046	0	0.0006	0.0169
C_8-C_9	0.0324	0.0087	0.0006	0	0.0111
C_{10+}	0.0779	0.0384	0.0169	0.0111	0

production, as illustrated in Figure 4(b) where only fluid-wall interaction is considered, the entire phase envelope is suppressed as the pore size decreases. Especially, considering fluid-wall interaction also reduces the critical point instead of considering only the capillary pressure. As the pore size decreases, the critical point and bubble point pressure become smaller. The phase envelope at 50 nm is almost the same as that of bulk phase, whereas the critical pressure at 5 nm is suppressed by 8.3%. This is because when the pore size decreases, the interaction between fluid molecules and pore wall increases. As can be seen in Figure 4(c) where only adsorption effect is considered, it's similar to just considering fluid-wall interaction. It can be seen from the Figures 4(a)–4(c) that the effect of capillary pressure, fluid-wall interaction and adsorption effect on the phase behavior in nanopores cannot be ignored.

By considering capillary pressure, fluid-wall interaction, and adsorption effect together, the P-T phase envelope of the Bakken tight oil reservoir at various pore sizes is plotted in Figure 4(d). It is illustrated that the phase envelope tends to move downward with the decrease of pore size. The critical point is reduced and the dew point curve shrinks compared with the phase envelope that only considers capillary pressure. The bubble point curve shrinks further than the phase envelope that considers only fluid-wall interaction or adsorption effect.

3.2.2. Bubble Point Pressure. The bubble point pressures at different pore sizes are calculated. Figure 5 describes the bubble point pressure at the reservoir temperature of 230°F and compares the nanopore confinement on bubble point pressure with different pore sizes. As illustrated in Figure 6, the smaller the pore size, the more significant the nanopore confinement effect. When the pore size is smaller than 10 nm, significant changes can be observed. The bubble point pressure reduces to 1542 psi (19.1% smaller) when the pore size is 10 nm, and the bubble point pressure suppresses to 650 psi (65.9% smaller) as the pore size decreases to 2 nm. However, when the pore size is above 100 nm, the bubble point pressure approaches to the bulk fluids, and the nanopore confinement effect can be neglected.

3.2.3. Interfacial Tension and Capillary Pressure. In this section, the interfacial tension (IFT) and capillary pressure (P_c) in different radii under different pressures at the reservoir temperature of 230°F are calculated. As shown in Figure 6, as the pressure increases, the interfacial tension decreases. The interfacial tension is significantly affected by the existence of nanopore confinement. The smaller the pore size, the greater the interfacial tension decreases. As described by Figure 7, when the pressure increases, the capillary pressure also decreases. The smaller the pore size, the greater the capillary pressure. When the pressure is 1500 psi, the capillary pressure with pore size of 5 nm is more than 5 times that of the bulk phase. As the pressure is smaller, the multiple increases. Therefore, the nanopore confinement effect will lead to high capillary pressure which cannot be ignored in tight oil reservoirs.

4. Recovery Mechanisms of CO_2 Injection

The accepted recovery mechanisms of CO_2-EOR in conventional reservoirs are as follows: (1) reduction of the vapor and liquid phase interfacial tension towards achieving miscibility with the crude oil, (2) CO_2 dissolves into crude oil, leading to oil volume expansion and crude oil viscosity reduction, (3) CO_2 extraction of lighter hydrocarbons from the liquid phase, (4) CO_2 molecular diffusion, and (5) the sweep efficiency is improved, thereby enhancing the ultimate oil recovery [56, 57]. Because of these recovery mechanisms, CO_2 flooding can greatly improve oil recovery. However, CO_2 injection in unconventional reservoirs such as tight oil reservoirs has not attracted enough attention. A better understanding of the effect of nanopore confinement effect on recovery mechanisms will help to optimize the design strategy for CO_2 injection in tight oil reservoirs.

4.1. Minimum Miscible Pressure (MMP). Minimum miscible pressure (MMP) is an important factor to decide miscible flooding. It is defined as the minimum pressure where the injected gas and the oil phase have no obvious interface and then become miscible with each other [58]. A series of PVT and core flooding tests have validated that CO_2 is much easier to become miscible with crude oil than other gases including flue gas, natural gas, and nitrogen [59]. Based on the calculation of phase equilibrium, we obtain the MMP at different CO_2 injection ratios. As observed in Figure 8, the MMP decreases gradually with the increase of CO_2

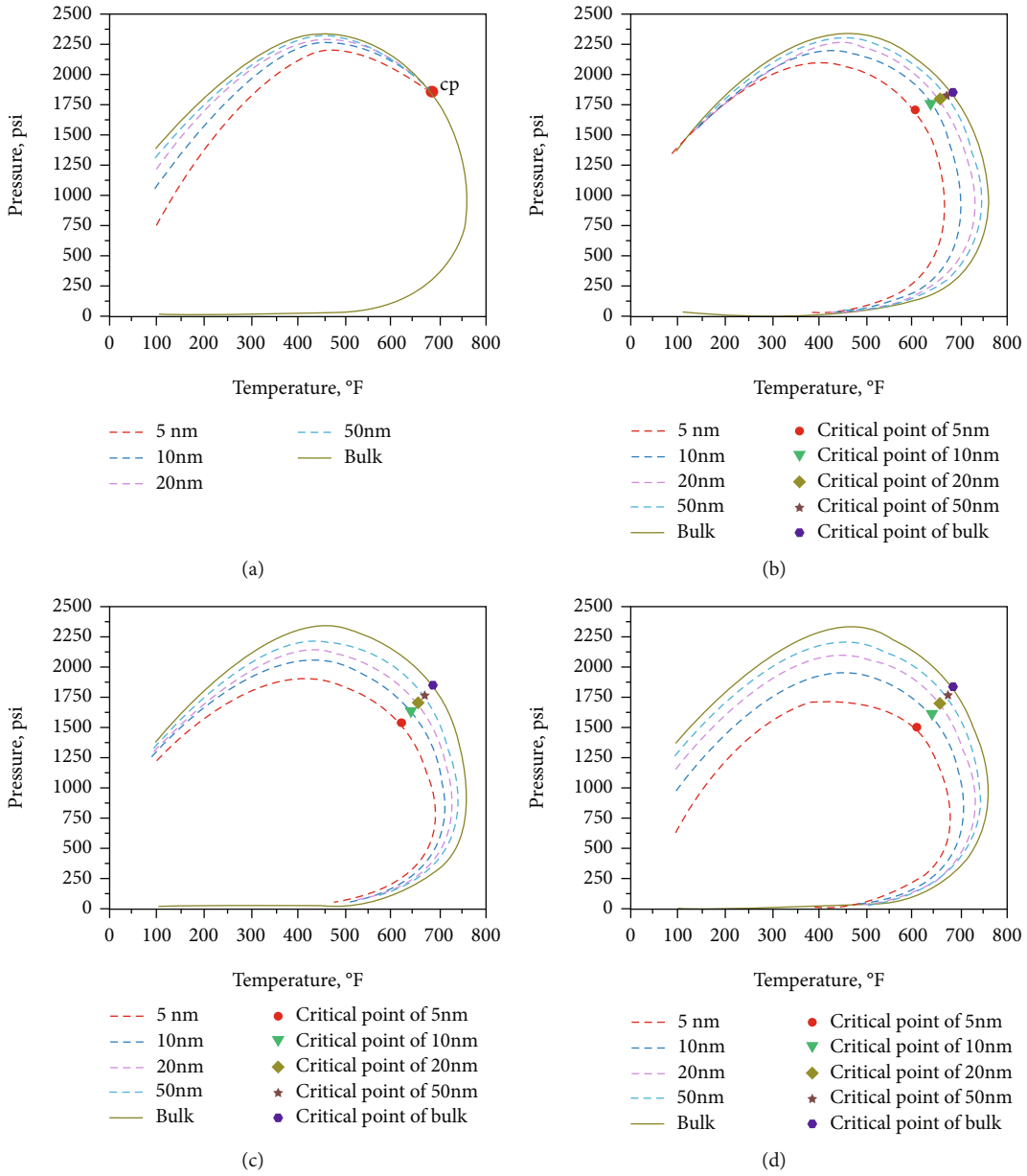

Figure 4: P-T phase envelope for Bakken tight oil reservoir at various pore sizes considering (a) capillary pressure, (b) fluid-wall interaction, (c) adsorption effect, and (d) nanopore confinement effect.

injection. When the gas injection ratio is 100%, the MMP decreased by 9.7% compared with the CO_2 injection ratio is 10%. In order to explore the influence of nanopore confinement effect on the MMP in tight oil reservoir, we also evaluated the MMP of 100% CO_2 injection at various pore sizes. As illustrated in Figure 9, the MMP tends to be lowered as the pore size decreases. When the pore size is 5 nm, the MMP decreased by 16.2% compared with the pore size is 100 nm.

4.2. CO_2 Solution Gas-Oil Ratio (GOR). The solution gas-oil ratio (GOR) is defined as the volume of gas at standard condition that evolves from the oil divided by the volume of oil at standard condition. CO_2 could dissolve into crude oil, leading to oil volume expansion and crude oil viscosity reduction. GOR is an important factor in evaluating the degree of CO_2 dissolution. We calculate the CO_2 solution gas-oil ratio of Bakken tight oil versus pressure at various CO_2 injections at $T = 230^{\circ}$F as shown in Figure 10. It is obvious that the CO_2 solution gas-oil ratio increases with the increase of gas injection. When the gas injection ratio is 100%, the CO_2 solution gas-oil ratio is about 3 times that of the gas injection ratio is 30%. In order to explore the influence of nanopore confinement effect on the CO_2 solution gas-oil ratio in tight oil reservoir, we also evaluated the CO_2 solution gas-oil ratio of 100% CO_2 injection at various pore sizes. As illustrated in Figure 11, before CO_2 is completely dissolved into crude oil, the CO_2 solution gas-oil ratio increases with the decrease of pore size. It indicates that considering the influence of nanopore confinement

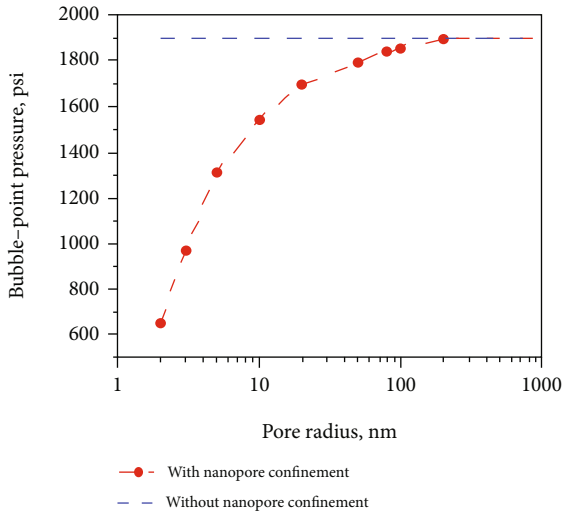

Figure 5: Bubble point pressure of the Bakken tight oil at various pore radii at $T = 230^{\circ}$F.

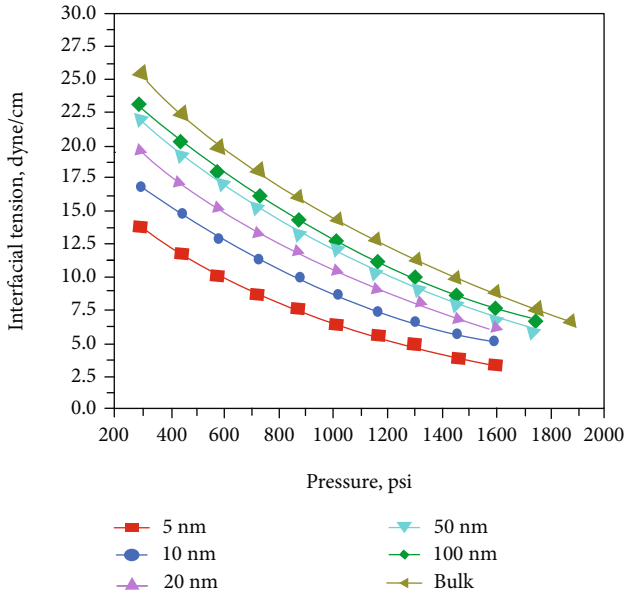

Figure 6: Interfacial tension of the Bakken tight oil versus pressure at various pore radii at $T = 230^{\circ}$F.

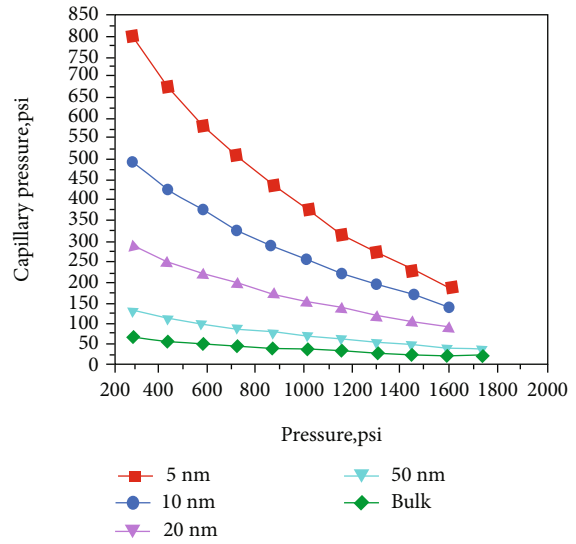

Figure 7: Capillary pressure of the Bakken tight oil versus pressure at various pore radii at $T = 230^{\circ}$F.

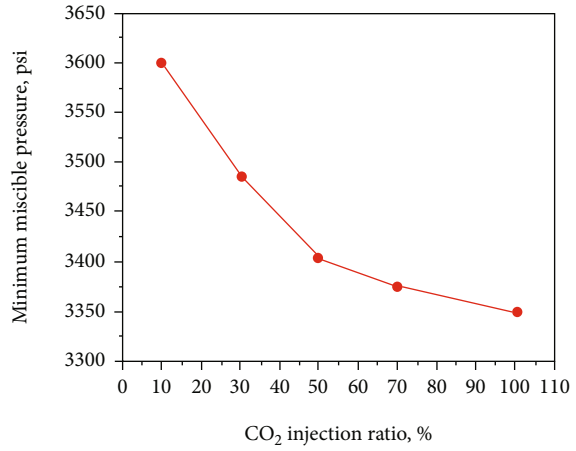

Figure 8: Minimum miscible pressure of the Bakken tight oil versus CO_2 injection.

effect, the amount of gas dissolved into crude oil increases, which will lead to the increase of the oil volume expansion and the decrease of the viscosity of crude oil, as shown in the following two sections. When the reservoir pressure is higher than the bubble point pressure, all the gas will be dissolved into the crude oil without free gas, and the value of solution gas-oil ratio will remain unchanged.

4.3. Oil Volume Expansion. CO_2 dissolves into the oil phase that causes the oil volume increase. The volumetric expansion capacity of crude oil can be characterized by the oil formation volume factor. The oil formation volume factor defines as the oil volume at reservoir condition divided by the oil volume at standard condition.

$$B_o = \frac{\left(n_L (V_m)_L\right)_{\mathrm{RC}}}{\left(n_L (V_m)_L\right)_{\mathrm{STD}}} \tag{27}$$

where n_L represents liquid phase mole fraction, $(V_m)_L$ represents liquid phase molar volume, RC represents reservoir condition, and STD represents standard condition.

Based on the phase equilibrium calculation, we calculate the oil formation volume factor of Bakken tight oil versus pressure at various CO_2 injections at $T = 230^{\circ}$F. As shown in Figure 12, it is obvious that the oil formation volume factor increases with the increase of gas injection. When the CO_2 injection ratio is 100%, the oil formation volume factor increased by 31.9% compared with that without CO_2 injection at pressure 4351.2 psi. This can be also explained by the variation trend of CO_2 solution gas-oil ratio in the upper section. In order to explore the influence of nanopore confinement effect on the oil formation volume in tight oil

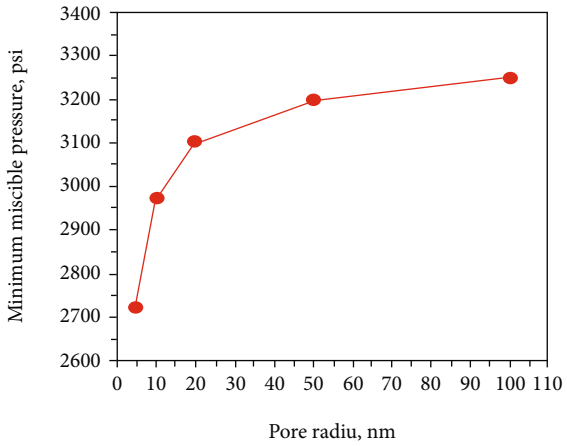

Figure 9: Minimum miscible pressure of the Bakken tight oil versus pore size.

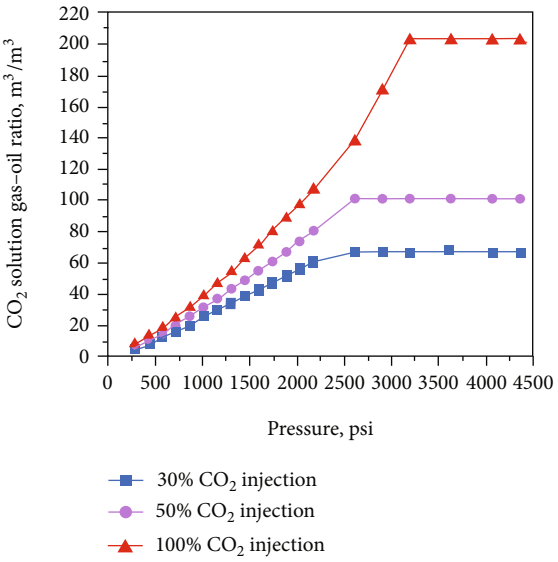

Figure 10: CO_2 solution gas-oil ratio of the Bakken tight oil versus pressure at various CO_2 injections at $T = 230^{\circ}$F.

reservoir, we also evaluate the oil formation volume factor of Bakken tight oil versus pressure at various pore radii at $T = 230^{\circ}$F. As illustrated in Figure 13, the oil formation volume factor of the oil increases as the pore size decreases. When the pore size decreases from infinity to 50 nm, 20 nm, 10 nm, and 5 nm, the increment of oil formation volume factor at pressure 4351.2 psi is almost 1.5%, 5.9%, 9.2%, and 14.7%.

4.4. Viscosity reduction. The oil viscosity is calculated by the Jossi-Stiel-Thodos (JST) model [60, 61].

$$\left[(\mu - \mu^*) + 10^{-4}\right]^{1/4} = a_0 + a_1\rho_r + a_2\rho_r^2 + a_3\rho_r^3 + a_4\rho_r^4, \quad (28)$$

where μ is the viscosity of crude oil under formation conditions, and the values of a_0, a_1, a_2, a_3, and a_4 are 0.1023, 0.023364, 0.058533, -0.040758, and 0.0093324, respectively.

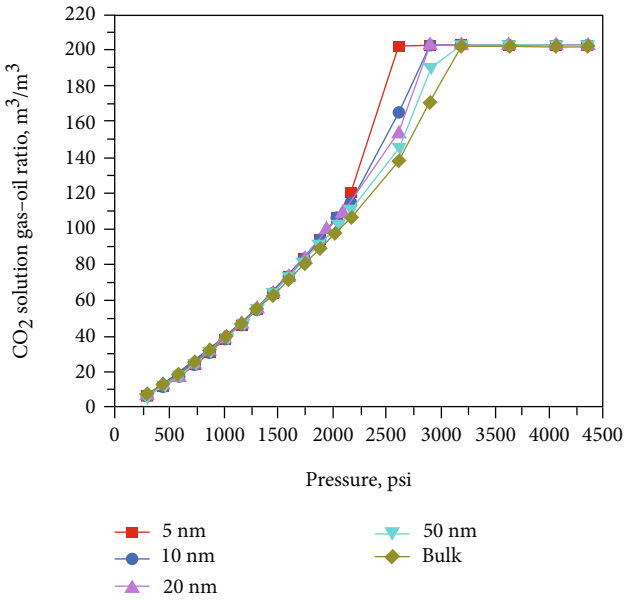

Figure 11: CO_2 solution gas-oil ratio of the Bakken tight oil versus pressure at various pore radii at $T = 230^{\circ}$F.

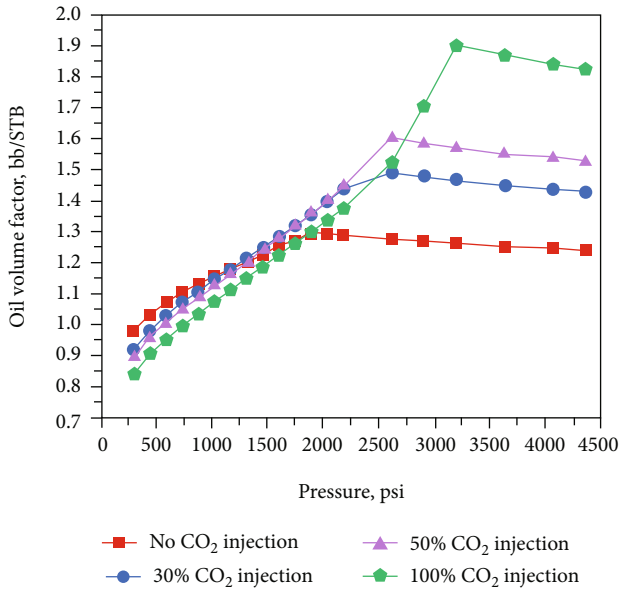

Figure 12: Oil volume factor of the Bakken tight oil versus pressure at various CO_2 injections at $T = 230^{\circ}$F.

ρ_r is defined as

$$\rho_r = \rho_L \left[\sum_{i=1}^{N_c} x_i V_{ci}\right]^{1/\alpha}, \quad (29)$$

where V_{ci} is a critical volume of component i, and the value of α is 1.

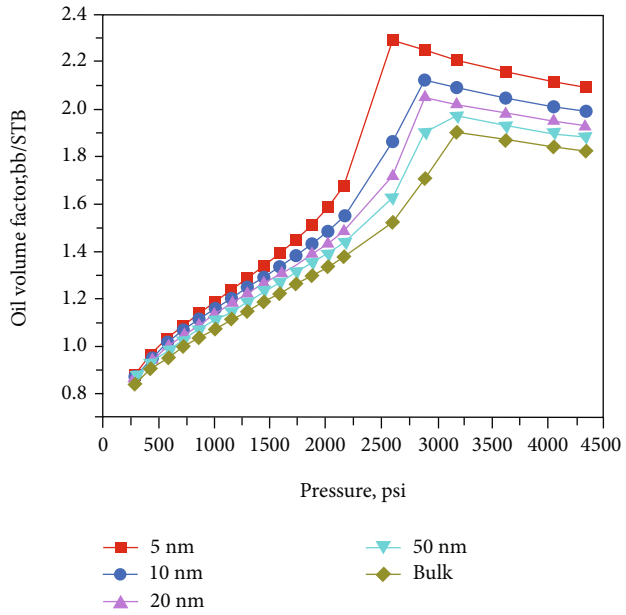

Figure 13: Oil volume factor of the Bakken tight oil versus pressure at various pore radii at $T = 230^{\circ}$F.

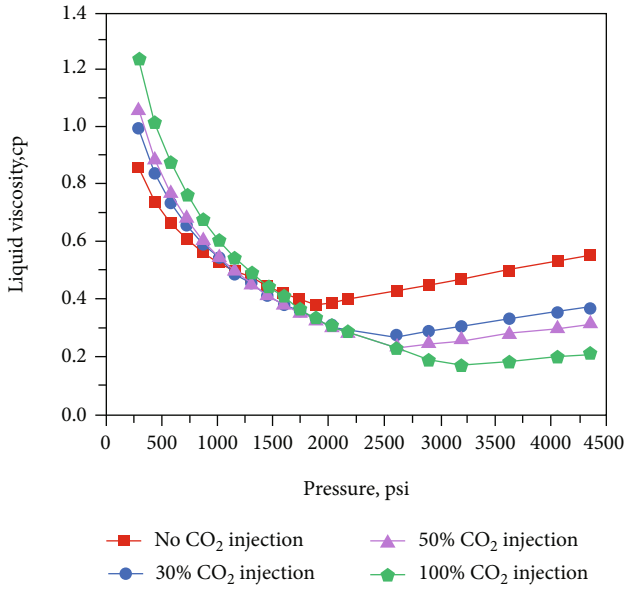

Figure 14: Oil viscosity of the Bakken tight oil versus pressure at various CO_2 injections at $T = 230^{\circ}$F.

The viscosity parameters of the mixture ξ are calculated by the following formula:

$$\xi = \left(\sum_{i=1}^{N_c} x_i T_{ci}\right)^{1/6} \left(\sum_{i=1}^{N_c} x_i M_i\right)^{-1/2} \left(\sum_{i=1}^{N_c} x_i P_{ci}\right)^{-2/3}. \quad (30)$$

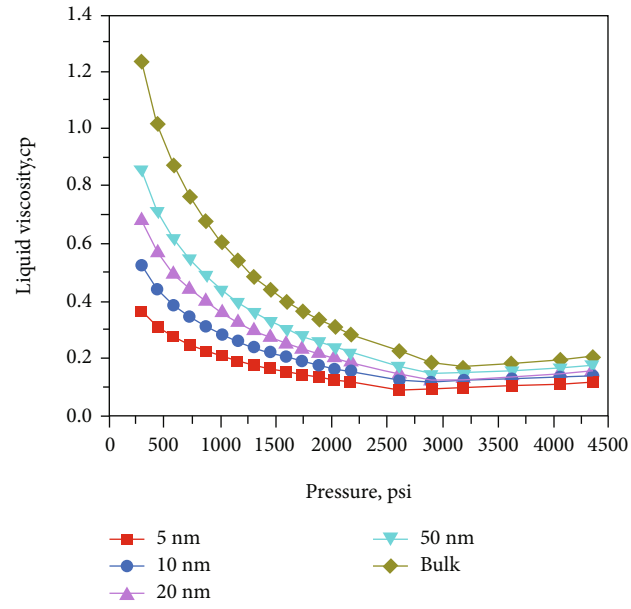

Figure 15: Oil viscosity of the Bakken tight oil versus pressure at various pore radii at $T = 230^{\circ}$F.

μ^* is defined as

$$\mu^* = \frac{\sum_{i=1}^{N_c}\left(x_i \mu_i^* M_i^{1/2}\right)}{\sum_{i=1}^{N_c}\left(x_i M_i^{1/2}\right)}. \quad (31)$$

μ_i^* can be calculated by the Stiel-Thodos formula:

$$\mu_i^* \xi_i = \begin{bmatrix} 4.610 T_{ri}^{0.618} - 2.04 e^{-0.449 T_{ri}} \\ +1.94 e^{-4.058 T_{ri}} + 0.1 \end{bmatrix} \times 10^{-4}, \quad (32)$$

where $\xi_i = T_{ci}^{1/6} M_i^{1/2} P_{ci}^{2/3}$, $T_{ri} = T/T_{ci}$.

Based on the phase equilibrium calculation, we calculate oil viscosity of the Bakken tight oil versus pressure at various CO_2 injections at $T = 230^{\circ}$F. As shown in Figure 14, it is obvious that the viscosity decreases with the increase of gas injection. When the CO_2 injection ratio is 100%, the oil viscosity decreased by 62.4% compared with that without CO_2 injection at pressure 4351.2 psi. This can be explained by the variation trend of CO_2 solution gas-oil ratio in the upper section. Hence, CO_2 has obvious viscosity reduction effect. In order to explore the influence of nanopore confinement effect on the oil viscosity in tight oil reservoir, we also evaluate the oil viscosity of Bakken tight oil versus pressure at various pore radius at $T = 230^{\circ}$F. As illustrated in Figure 15, the viscosity of the oil reduces as the pore size decreases. When the pore size decreases from infinity to 50 nm, 20 nm, 10 nm, and 5 nm, the suppression of oil viscosity at corresponding bubble point pressure are almost 13.4%, 24.8%, 33.8%, and 42.8%. It indicates that considering the influence of nanopore confinement effect, the oil mobility could be increased.

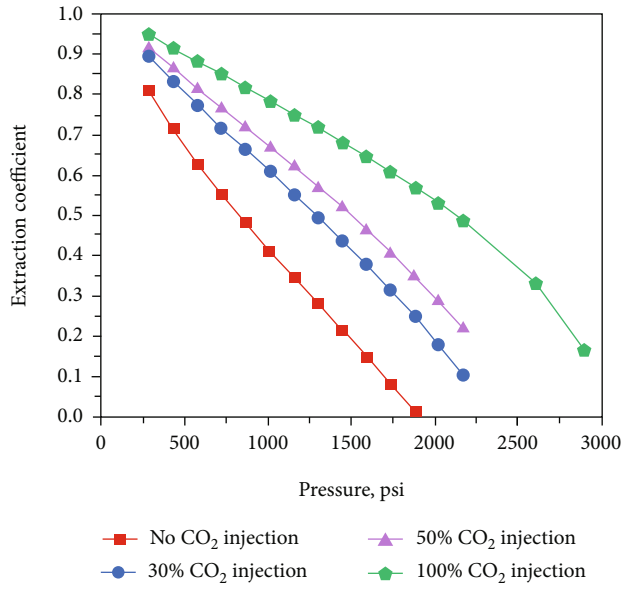

Figure 16: Extraction coefficient of lighter hydrocarbons for the Bakken tight oil versus pressure at various CO_2 injections at $T = 230^{\circ}$F.

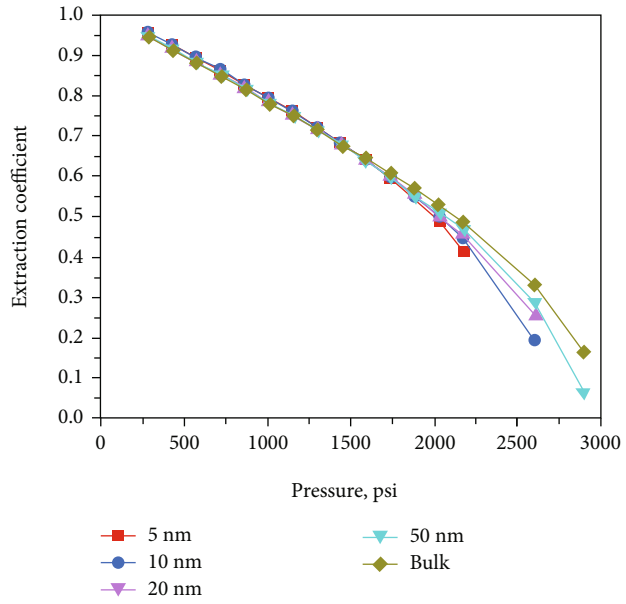

Figure 17: Extraction coefficient of lighter hydrocarbons for the Bakken tight oil versus pressure at various pore radii at $T = 230^{\circ}$F.

4.5. Extraction of Lighter Hydrocarbons. Many experiments and simulations have shown that the content of light components in the oil produced after CO_2 injection increases while the content of heavy components decreases. The mass transfer between CO_2 and formation crude oil results in substantial physical changes of the system.

The extraction coefficient β_e of lighter hydrocarbon is defined as

$$\beta_e = \frac{n_V y_i}{z_i}. \tag{33}$$

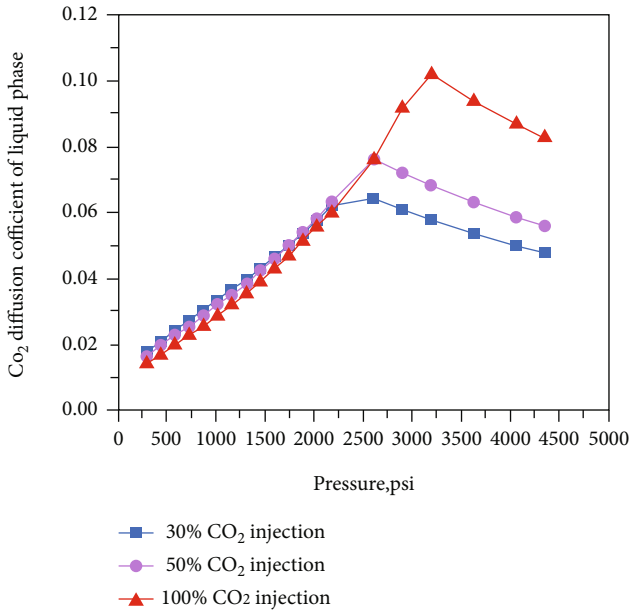

Figure 18: CO_2 diffusion coefficient of liquid phase for the Bakken tight oil versus pressure at various CO_2 injection at $T = 230^{\circ}$F.

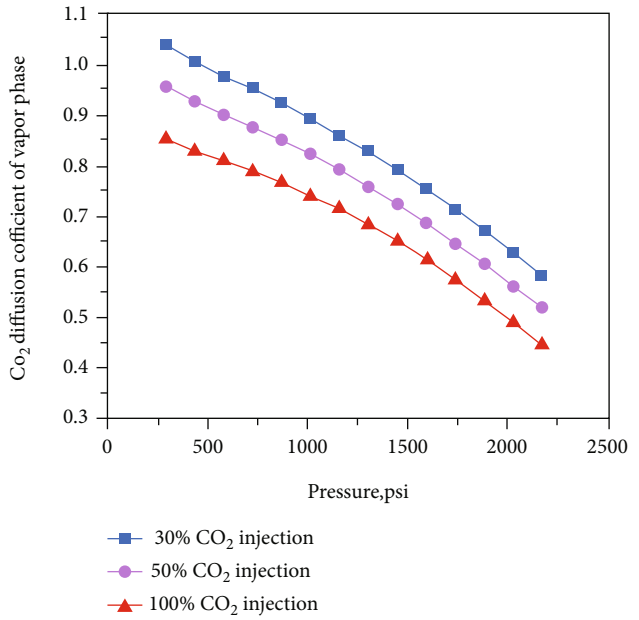

Figure 19: CO_2 diffusion coefficient of vapor phase for the Bakken tight oil versus pressure at various CO_2 injections at $T = 230^{\circ}$F.

Based on the phase equilibrium calculation, we calculate the extraction coefficient of lighter hydrocarbon of the Bakken tight oil versus pressure at various CO_2 injections at $T = 230^{\circ}$F. As shown in Figure 16, it is obvious that the extraction coefficient of lighter hydrocarbon increases with the increase of gas injection. This can be explained by the following mechanisms: Carbon dioxide dissolves and the liquid phase is relatively light, which contributes to the evaporation of light components and the enrichment of gas phase. Because the gas phase is enriched and the liquid phase is relatively light, the difference of components in the gas and

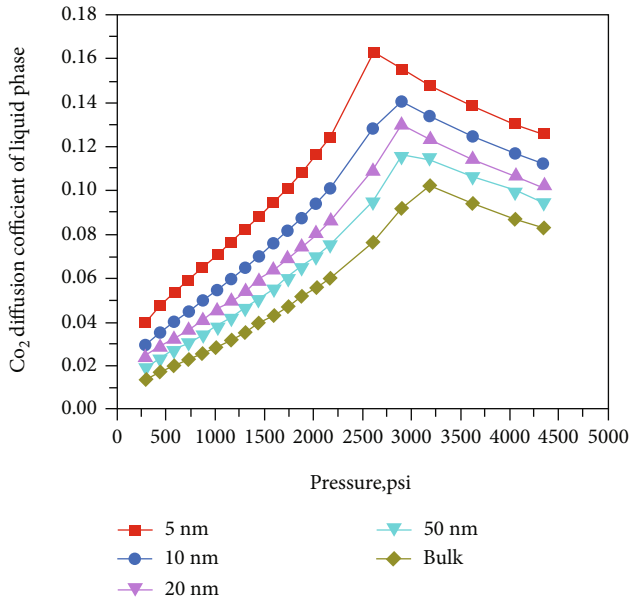

Figure 20: CO_2 diffusion coefficient of liquid phase for Bakken tight oil versus pressure at various pore radii at $T = 230^{\circ}$F.

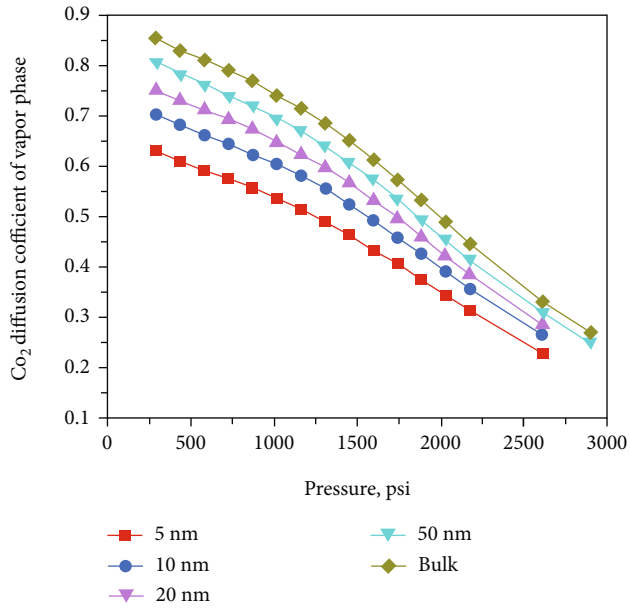

Figure 21: CO_2 diffusion coefficient of vapor phase for Bakken tight oil versus pressure at various pore radii at $T = 230^{\circ}$F.

liquid phase is relatively small. According to the similar compatibility principle, the mass transfer capacity of gas-liquid system is enhanced, and the result is that the enriched gas further extracts the light hydrocarbon and the intermediate hydrocarbon components of crude oil to form the rich hydrocarbon phase. Therefore, the CO_2 extraction of lighter hydrocarbons is conducive to improving the properties of crude oil and enhancing oil recovery.

In order to explore the influence of nanopore confinement effect on the oil formation volume in tight oil reservoir, we also evaluate the extraction coefficient of lighter hydrocarbon of the Bakken tight oil versus pressure at various pore radii at $T = 230^{\circ}$F. As illustrated in Figure 17, the extraction coefficient of lighter hydrocarbon slightly reduces as the pore size decreases. It indicates that considering nanopore confinement effect seems to have a slightly reduced effect on extraction of lighter hydrocarbons.

4.6. Molecular Diffusion. Molecular diffusion is one of favorable mechanism factors for oil recovery, especially for tight oil reservoirs. The flow velocity is low in tight oil reservoirs with low matrix permeability that the relative contribution of molecular diffusion becomes more significant compared with molecular diffusion in conventional reservoirs. Two empirical correlations frequently applied are by the Wilke-Chang correlation [62] and the Sigmund correlation [63]. In this study, we employed Wilke -Chang equation to estimate the CO_2 diffusion coefficient as

$$D_{ik} = \frac{7.4 \times 10^8 (\phi M_i)^{1/2} T}{\mu_k V_{kb}^{0.6}}, \tag{34}$$

where D_{ik} represents the diffusion coefficient of component i in phase k, M_{CO2} is the molar mass of component i, T is the temperature of system, μ_k is viscosity of phase k, V_{kb} is the critical volume of phase k under the bubble point, and ϕ is association factor, which depends on the properties of the solvent itself. If ethanol is the solvent, it has a value of 1.5. However, the calculation error is larger for nonassociative systems, and Sun and Chen [64] deduced the relationship between the association factor and temperature through the free volume theory as follows:

$$\phi(T) = 3.97 - 3.92 \times 10^{-3} T. \tag{35}$$

Based on the phase equilibrium calculation, we evaluate the CO_2 diffusion coefficient for the liquid and vapor phases at various CO_2 injections at $T = 230^{\circ}$F. As shown in Figures 18 and 19, CO_2 diffusion coefficient of the liquid phase increases with the increase of gas injection while.

CO_2 diffusion coefficient of vapor phase decreases with the increase of gas injection. In order to explore the influence of nanopore confinement effect on the CO_2 diffusion coefficient in tight oil reservoir, we also evaluate the CO_2 diffusion coefficient of Bakken tight oil versus pressure at various pore radii at $T = 230^{\circ}$F. As illustrated in Figures 20 and 21, the CO_2 diffusion coefficient is also different for the liquid phase and vapor phase under nanopore confinement effect. CO_2 diffusion coefficient for the liquid phase is larger in smaller pores whereas CO_2 diffusion coefficient for the vapor phase is smaller.

5. Summary and Conclusions

(1) An efficient model is proposed to calculate phase behavior in tight oil reservoir with capillary pressure, fluid-wall interaction and adsorption effect in this work. Fluid-wall interaction and adsorption effect are introduced to modify the PR-EOS, and capillary

pressure is used to modify the flash calculation for phase equilibrium calculation. The model has been verified against commercial software (CMG-Winprop) and experimental data with bulk fluids and confined fluids. The results show that the nanopore confinement effects including capillary pressure, fluid-wall interaction, and adsorption effect are significant when the pore radius reduces to the orders of nanometers

(2) For the Bakken tight oil reservoir, nanopore confinement effects impose an overall shrinkage to the *P-T* phase envelope. Capillary pressure lowers bubble point curve as the pore size decreases. Fluid-wall interaction and adsorption effect suppress the entire phase envelope as the pore size decreases. Especially, they reduce the critical point instead of capillary pressure. The bubble point pressure of Bakken oil is suppressed by 19.1% when the pore size is 10 nm under nanopore confinement effect compared with the counterpart case without pore proximity. It is reduced by 65.9% when the pore size is 2 nm. As the pore size decreases, the IFT decreases whereas the capillary pressure increases obviously

(3) The recovery mechanisms for CO_2 injection are also investigated in the Bakken tight oil reservoir from different respects. Results show that the MMP decreases gradually with the increase of CO_2 injection. When the gas injection ratio is 100%, the MMP decreased by 9.7% compared with the CO_2 injection ratio is 10%. On this basis, the effect of nanopore confinement on the MMP for CO_2 injection is also calculated. Results indicate that under the nanopore confinement effect, the MMP will decrease, resulting in the suppression of the resistance of fluid transport. Hence, it will be easier to reach miscibility and improve the well performance. Besides, as the increase of CO_2 injection, the CO_2 solubility will increase, the volume of crude oil expands, and the oil viscosity will decrease. With the nanopore confinement effect, the CO_2 solution gas-oil ratio and the oil formation volume factor of the oil increase with the decrease of pore size. In turn, the oil viscosity reduces as the pore size decreases. Furthermore, the extraction coefficient of lighter hydrocarbon increases with the increase of gas injection. With the nanopore confinement effect, the extraction coefficient of lighter hydrocarbon slightly reduces as the pore size decreases. It indicates that considering nanopore confinement effect seems to have a slightly reduced effect on extraction of lighter hydrocarbons. The CO_2 diffusion coefficients for liquid phase and vapor phase are different in that CO_2 diffusion coefficients for liquid phase increase with the increase of gas injection while CO_2 diffusion coefficient of vapor phase decreases. On this basis, we also evaluate the effect of nanopore confinement on the CO_2 diffusion. Results show that CO_2 diffusion coefficient are also different for liquid phase and vapor phase under nanopore confinement effect. CO_2 diffusion coefficient for liquid phase is larger in smaller pores whereas CO_2 diffusion coefficient for vapor phase is smaller

(4) An efficient model is proposed to calculate phase behavior in tight oil reservoir with capillary pressure, fluid-wall interaction, and adsorption effect simultaneously. However, the model does not take the effect of water on phase behavior into account, and the pore size distribution is also not considered. Further extensive research on these will continue to investigate

Appendix

The modified PR-EOS is given as follows:

$$P = \frac{RT}{V'_m - b} - \frac{a - c}{V'_m\left(V'_m + b\right) + b\left(V'_m - b\right)}. \tag{A.1}$$

The first and second derivatives of pressure with respect to volume at critical point are yielded:

$$\left(\frac{\partial P}{\partial V}\right)_{T=T_c} = -\frac{\alpha RT_c}{(\alpha V_c - \mathrm{b})^2} + \frac{2\alpha(a - \mathrm{c})(\alpha V_c + b)}{[\alpha V_c(\alpha V_c + b) + b(\alpha V_c - b)]^2} = 0, \tag{A.2}$$

$$\left(\frac{\partial^2 P}{\partial V^2}\right)_{T=T_c} = \frac{2\alpha^2 RT_c}{(\alpha V_c - \mathrm{b})^3} + \frac{2\alpha^2(a - \mathrm{c})[b(\alpha V_c - \mathrm{b}) - (\alpha V_c + b)(3\alpha V_c + 4b)]}{[\alpha V_c(\alpha V_c + b) + b(\alpha V_c - b)]^3} = 0. \tag{A.3}$$

From Equation (A.2), it is given as

$$\frac{RT_c}{(\alpha V_c - \mathrm{b})^3} = \frac{2(a - \mathrm{c})(\alpha V_c + b)}{[\alpha V_c(\alpha V_c + b) + b(\alpha V_c - b)]^2(\alpha V_c - \mathrm{b})}. \tag{A.4}$$

Imposing Equation (A.4) on Equation (A.3), it is yielded as

$$\frac{2(\alpha V_c + b)}{\alpha V_c - b} = \frac{(\alpha V_c + b)(3\alpha V_c + 4b) - b(\alpha V_c - b)}{(\alpha V_c(\alpha V_c + b) + b(\alpha V_c - b))}. \tag{A.5}$$

It can be rewritten as

$$-(\alpha V_c + b)(\alpha V_c - \mathrm{b})(3\alpha V_c + 2b) + 2\alpha V_c(\alpha V_c + b)^2 + b(\alpha V_c - b)^2 = 0. \tag{A.6}$$

We assume $b = k\alpha V_c$, and Equation (A.6) can be rewritten as

$$3k^3 + 3k^2 + 3k - 1 = 0. \tag{A.7}$$

Solving for k could obtain $k = 0.25308$.

$$b = 0.25308\alpha V_c. \tag{A.8}$$

Imposing Equation (A.8) on Equation (A.2), it is written as

$$-\frac{RT_c}{(1-k)^2} + \frac{2(a-c)(1+k)}{(\alpha V_c)[(1+k)+k(1-k)]^2} = 0. \tag{A.9}$$

Thus,

$$a - c = \frac{RT_c(\alpha V_c)[(1+k)+k(1-k)]^2}{2(1+k)(1-k)^2} = 1.48742\alpha RT_c V_c. \tag{A.10}$$

Applying Equation (A.1) to the critical point and substituting Equations (A.8) and (A.10) into Equation (A.1), it is obtained as

$$\frac{P_c V_c}{RT_c} = \frac{0.30740}{\alpha}. \tag{A.11}$$

b is the van der Waals covolume, and the relationship between b and V_c should be obtained from the traditional PR-EOS,

$$b = 0.25308 V_c. \tag{A.12}$$

From Equations (A.10), (A.11), and (A.12)), the parameters a and b are given as follows:

$$\begin{aligned} a - c &= 0.45724\frac{R^2 {T_C}^2}{P_c}, \\ b &= 0.07780\frac{RT_c}{\alpha P_c}. \end{aligned} \tag{A.13}$$

Nomenclature

P: System pressure
T: System temperature
R: Gas constant
V_m: Molar volume
a: "Attraction" parameter
b: "Repulsion" parameter
c: Fluid-wall interaction effect coefficient
α: Adsorption effect coefficient
P_{CC}: The critical pressure determined by the modified PR-EOS
T_{CC}: The critical temperature determined by the modified PR-EOS
ΔP: The dimensionless shifts of critical pressure
ΔT: The dimensionless shifts of critical temperature
r_p: Pore size
σ_{LJ}: Lennard-Jones molecular size parameter
N_c: The number of components
f_i^L: Fugacity of component i in the liquid phase
f_i^V: Fugacity of component i in the vapor phase
x_i: Mole fraction of component i in the liquid phase
y_i: Mole fraction of component i in the vapor phase
z_i: Overall mole fraction of component i
φ_i^L: Fugacity coefficient of component i in the liquid phase
φ_i^V: Fugacity coefficient of component i in the vapor phase
n_L: Overall number of moles in liquid phase
n_V: Overall number of moles in vapor phase
K_i: Phase equilibrium ratio of component i
P_{cap}: Capillary pressure
σ: Interfacial tension
θ: Contact angle
ρ_L: Density of liquid phase
ρ_V: Density of vapor phase
$[P]_i$: The parachor of component i
Z: The compressibility factor
B_o: Oil formation volume factor
μ: Viscosity of crude oil
V_{ci}: Critical volume of component i
β_e: The extraction coefficient
D_{ik}: The diffusion coefficient of component i in phase k
RC: Reservoir condition
STD: Standard condition.

Data Availability

All the data supporting this study can be found in the manuscript.

Conflicts of Interest

The authors declare that there is no conflict of interest regarding the publication of this paper.

Acknowledgments

This work was supported by the National Nature Science Foundation of China (51674010). We would like to acknowledge Computer Modeling Group Ltd. for providing the CMG software for this study of example validation.

References

[1] BP, *BP Energy Outlook*, BP, 2019.
[2] EIA, "US energy information administration," 2019, https://www.eia.gov/.
[3] L. Wang, E. Parsa, Y. Gao, J. T. Ok, K. Neeves, and X. Yin, "Experimental study and modeling of the effect of nanoconfinement on hydrocarbon phase behavior in un- conventional reservoirs," in *Presented at the SPE western North American and rocky mountain joint regional meeting*, pp. 1–8, Denver, CO, USA, 2014.
[4] S. Salahshoor, M. Fahes, and C. Teodoriu, "A review on the effect of confinement on phase behavior in tight formations," *Journal of Natural Gas Science and Engineering*, vol. 51, pp. 89–103, 2018.
[5] Q. Feng, S. Xu, X. Xing, W. Zhang, and S. Wang, "Advances and challenges in shale oil development: a critical review,"

Advances in Geo-Energy Research, vol. 4, no. 4, pp. 406–418, 2020.

[6] S. Sun and T. Zhang, "A 6M digital twin for modelling and simulation for subsurface reservoirs," *Advances in Geo-Energy Research*, vol. 4, pp. 349–351, 2020.

[7] S. Roy, R. Raju, H. Chuang, B. Cruden, and M. Meyyappan, "Modeling gas flow through microchannels and nanopores," *Journal of Applied Physics*, vol. 93, no. 8, pp. 4870–4879, 2003.

[8] P. H. Nelson, "Pore-throat sizes in sandstones, tight sandstones, and shales," *AAPG Bulletin*, vol. 93, no. 3, pp. 329–340, 2009.

[9] J. Wang, S. Wu, Q. Li, J. Zhang, and Q. Guo, "Characterization of the pore-throat size of tight oil reservoirs and its control on reservoir physical properties: a case study of the Triassic tight sandstone of the sediment gravity flow in the Ordos Basin, China," *Journal of Petroleum Science and Engineering*, vol. 186, article 106701, 2019.

[10] Y. Wang, B. Yan, and J. Killough, "Compositional modeling of tight oil using dynamic nanopore properties," in *Paper SPE 166267 presented at SPE Annual Technical Conference and Exhibition*, pp. 1–13, New Orleans, LA, USA, 2013.

[11] B. Nojabaei, R. T. Johns, and L. Chu, "Effect of capillary pressure on phase behavior in tight rocks and shales," in *Paper SPE 159258 presented at the SPE Annual Technical Conference and Exhibition*, pp. 281–289, San Antonio, TX, USA, 2012.

[12] S. Luo, H. Nasrabadi, and J. L. Lutkenhaus, "Effect of confinement on the bubble points of hydrocarbons in nanoporous media," *AICHE Journal*, vol. 62, no. 5, pp. 1772–1780, 2016.

[13] S. Luo, J. L. Lutkenhaus, and H. Nasrabadi, "Experimental study of pore size distribution effect on phase transitions of hydrocarbons in nanoporous media," *Fluid Phase Equilibria*, vol. 487, p. 8015, 2019.

[14] B. Pinho, S. Girardon, F. Bazer-Bachi, G. Bergeot, S. Marre, and C. Aymonier, "A microfluidic approach for investigating multicomponent system thermodynamics at high pressures and temperatures," *Lab on a Chip*, vol. 14, no. 19, pp. 3843–3849, 2014.

[15] V. R. Choudhary and K. Mantri, "Temperature-programmed desorption of benzene on mesoporous Si-MCM-41, Na-AlSi-MCM-41, and H-AlSi-MCM-41," *Langmuir*, vol. 16, pp. 8024–8030, 2020.

[16] H. Xu, "Probing nanopore structure and confined fluid behavior in shale matrix: a review on small-angle neutron scattering studies," *International Journal of Coal Geology*, vol. 217, article 103325, 2020.

[17] H. Cho, M. H. Bartl, and M. Deo, "Bubble point measurements of hydrocarbon mixtures in mesoporous media," *Energy Fuels*, vol. 31, no. 4, pp. 3436–3444, 2017.

[18] G. Günther, J. Prass, O. Paris, and M. Schoen, "Novel insights into nanopore deformation caused by capillary condensation," *Physical Review Letters*, vol. 101, no. 8, article 086104, 2008.

[19] J. Zhong, S. Talebi, Y. Xu, Y. Pang, F. Mostowfi, and D. Sinton, "Fluorescence in sub-10 nm channels with an optical enhancement layer," *Lab on a Chip*, vol. 18, no. 4, pp. 568–573, 2018.

[20] Y. Liu, X. Dong, Z. Chen, Y. Hou, Q. Luo, and Y. Chen, "A novel experimental investigation on the occurrence state of fluids in microscale pores of tight reservoirs," *Journal of Petroleum Science and Engineering*, vol. 196, article 107656, 2020.

[21] S. Wang, Q. Feng, M. Zha et al., "Molecular dynamics simulation of liquid alkane occurrence state in pores and slits of shale organic matter," *Petroleum Exploration and Development*, vol. 42, no. 6, pp. 844–851, 2015.

[22] Z. Jin and A. Firoozabadi, "Thermodynamic modeling of phase behavior in shale media," *SPE Journal*, vol. 21, no. 1, pp. 190–207, 2016.

[23] Y. Zhang, W. Yu, K. Sepehrnoori, and Y. Di, "Investigation of nanopore confinement on fluid flow in tight reservoirs," *Journal of Petroleum Science and Engineering*, vol. 150, pp. 265–271, 2017.

[24] L. Li and J. J. Sheng, "Nanopore confinement effects on phase behavior and capillary pressure in a Wolfcamp shale reservoir," *Journal of Taiwan Institute of Chemical Engineers*, vol. 78, pp. 317–328, 2017.

[25] Q. Yang, P. Sun, L. Fumagalli et al., "Capillary condensation under atomic-scale confinement," *Nature*, vol. 588, no. 7837, pp. 250–253, 2020.

[26] L. Travalloni, M. Castier, F. W. Tavares, and S. I. Sandler, "Thermodynamic modeling of confined fluids using an extension of the generalized van der Waals theory," *Chemical Engineering Science*, vol. 65, no. 10, pp. 3088–3099, 2010.

[27] G. Yang, Z. Fan, and X. Li, "Determination of confined fluid phase behavior using extended Peng-Robinson equation of state," *Chemical Engineering Journal*, vol. 378, pp. 122–132, 2019.

[28] X. Dong, H. Liu, K. Wu et al., "Confined behavior of CO_2/hydrocarbon system in nanopores of tight and shale rocks," in *Unconventional Resources Technology Conference. Society of Exploration Geophysicists*, pp. 1–14, Denver, Colorado, USA, 2019.

[29] X. Cui, E. Yang, K. Song, and J. Huang, "Phase equilibrium of hydrocarbons confined in nanopores from a modified Peng-Robinson equation of state," in *SPE Annual Technical Conference and Exhibition, Society of Petroleum Engineers*, pp. 1–21, Dallas, Texas, USA, 2018.

[30] D. R. Sandoval, W. Yan, M. L. Michelsen, and E. H. Stenby, "Influence of adsorption and capillary pressure on phase equilibria inside shale reservoirs," *Energy & Fuels*, vol. 32, no. 3, pp. 2819–2833, 2018.

[31] Z. Song, Y. Song, J. Guo, Z. Zhang, and J. Hou, "Adsorption induced critical shifts of confined fluids in shale nanopores," *Chemical Engineering Journal*, vol. 385, article 123837, 2020.

[32] Y. Zhang, H. Lashgari, Y. di, and K. Sepehrnoori, "Capillary pressure effect on phase behavior of CO_2/hydrocarbons in unconventional reservoirs," *Fuel*, vol. 197, pp. 575–582, 2017.

[33] X. Zhang and W. Wang, "Square-well fluids in confined space with discretely attractive wall-fluid potentials: critical point shift," *Physical Review E*, vol. 74, no. 6, article 062601, 2006.

[34] K. Wu, Z. Chen, X. Li, and X. Dong, "Methane storage in nanoporous material at supercritical temperature over a wide range of pressures," *Scientific Reports*, vol. 6, no. 1, article 33461, 2016.

[35] Z. Jiang, L. Zhao, and D. Zhang, "Study of adsorption behavior in shale reservoirs under high pressure," *Journal of Natural Gas Science and Engineering*, vol. 49, pp. 275–285, 2018.

[36] K. Zhang, N. Jia, and L. Liu, "Adsorption thicknesses of confined pure and mixing fluids in nanopores," *Langmuir*, vol. 34, no. 43, pp. 12815–12826, 2018.

[37] A. Taghavinejad, M. Sharifi, E. Heidaryan, K. Liu, and M. Ostadhassan, "Flow modeling in shale gas reservoirs: a comprehensive review," *Journal of Natural Gas Science and Engineering*, vol. 83, article 103535, 2020.

[38] D. Y. Peng and D. B. Robinson, "A new two-constant equation of state," *Industrial and Engineering Chemistry Fundamentals*, vol. 15, no. 1, pp. 59–64, 1976.

[39] M. Fechtner and A. Kienle, "Efficient simulation and equilibrium theory for adsorption processes with implicit adsorption isotherms - ideal adsorbed solution theory," *Chemical Engineering Science*, vol. 177, pp. 284–292, 2018.

[40] A. A. Shapiro and E. H. Stenby, "Potential theory of multicomponent adsorption," *Journal of Colloid and Interface Science*, vol. 201, no. 2, pp. 146–157, 1998.

[41] R. S. Myong, "Gaseous slip models based on the Langmuir adsorption isotherm," *Physics of Fluids*, vol. 16, no. 1, pp. 104–117, 2004.

[42] A. Tarek, *Equation of State and PVT Analysis: Application for Improved Reservoir Modeling*, Gulf Publishing Company, 2nd edition, 2016.

[43] C. G. Burgess, D. H. Everett, and S. Nuttall, "Adsorption of carbon dioxide and xenon by porous glass over a wide range of temperature and pressure-applicability of the Langmuir case VI equation," *Langmuir*, vol. 6, no. 12, pp. 1734–1738, 1990.

[44] A. Vishnyakov, E. M. Piotrovskaya, E. N. Brodskaya, E. V. Votyakov, and Y. K. Tovbin, "Critical properties of Lennard-Jones fluids in narrow slit-shaped pores," *Langmuir*, vol. 17, no. 14, pp. 4451–4458, 2001.

[45] B. R. Didar and I. Y. Akkutlu, "Pore-size dependence of fluid phase behavior and properties in organic-rich shale reservoirs," in *SPE International Symposium on Oilfield Chemistry. Society of Petroleum Engineers*, pp. 1–19, Woodlands, Texas, USA, 2013.

[46] T. Pitakbunkate, P. Balbuena, G. J. Moridis, and T. A. Blasingame, "Effect of confinement on PVT properties of hydrocarbons in shale reservoirs," in *SPE Annual Technical Conference and Exhibition. Society of Petroleum Engineers*, pp. 1–16, Amsterdam, Netherlands, 2014.

[47] B. Jin and H. Nasrabadi, "Phase behavior of multi-component hydrocarbon systems in nano-pores using gauge-GCMC molecular simulation," *Fluid Phase Equilibria*, vol. 425, pp. 324–334, 2016.

[48] S. Luo, J. L. Lutkenhaus, and H. Nasrabadi, "Use of differential scanning calorimetry to study phase behavior of hydrocarbon mixtures in nano-scale porous media," *Journal of Petroleum Science and Engineering*, vol. 163, pp. 731–738, 2018.

[49] S. K. Singh, A. Sinha, G. Deo, and J. K. Singh, "Vapor-liquid phase coexistence, critical properties, and surface tension of confined alkanes," *Journal of Physical Chemistry C*, vol. 113, no. 17, pp. 7170–7180, 2009.

[50] S. P. Tan, X. Qiu, M. Dejam, and H. Adidharma, "Critical point of fluid confined in nanopores: experimental detection and measurement," *Journal of Physical Chemistry C*, vol. 123, no. 15, pp. 9824–9830, 2019.

[51] A. W. Islam, T. W. Patzek, and A. Y. Sun, "Thermodynamics phase changes of nanopore fluids," *Journal of Natural Gas Science and Engineering*, vol. 25, pp. 134–139, 2015.

[52] H. H. Rachford and J. D. Rice, "Procedure for use of electronic digital computers in calculating flash vaporization hydrocarbon equilibrium," *Journal of Petroleum Technology*, vol. 4, no. 10, pp. 19–30, 1952.

[53] A. W. Adamson, *Physical Chemistry of Surfaces*, John Wiley & Sons, 5th edition, 1990.

[54] K. S. Pedersen and P. L. Christensen, *Phase Behavior of Petroleum Reservoir Fluids*, CRC Press, 2007.

[55] W. Yu, H. R. Lashgari, K. Wu, and K. Sepehrnoori, "CO_2 injection for enhanced oil recovery in Bakken tight oil reservoirs," *Fuel*, vol. 159, pp. 354–363, 2015.

[56] B. Jia, J. S. Tsau, and R. Barati, "A review of the current progress of CO_2 injection EOR and carbon storage in shale oil reservoirs," *Fuel*, vol. 236, pp. 404–427, 2019.

[57] Z. Song, Y. Song, Y. Li, B. Bai, K. Song, and J. Hou, "A critical review of CO_2 enhanced oil recovery in tight oil reservoirs of North America and China," *Fuel*, vol. 276, article 118006, 2020.

[58] O. O. Adekunle and B. T. Hoffman, "Minimum miscibility pressure studies in the Bakken," in *Paper SPE 169077 presented at the SPE Improved Oil Recovery Symposium*, pp. 1–16, Tulsa, OK, USA, 2014.

[59] S. Wu, Z. Li, and H. K. Sarma, "Influence of confinement effect on recovery mechanisms of CO_2-enhanced tight-oil recovery process considering critical properties shift, capillarity and adsorption," *Fuel*, vol. 262, article 116569, 2020.

[60] P. Yoonm and G. Thodos, "Viscosity of nonpolar gaseous mixtures at normal pressures," *AICHE Journal*, vol. 16, no. 2, pp. 300–304, 1970.

[61] D. K. Fong and L. X. Nghiem, "A viscosity model for reservoir fluid," *Computer Modeling Group Research Report*, 1980.

[62] C. R. Wilke and P. Chang, "Correlation of diffusion coefficients in dilute solutions," *AICHE Journal*, vol. 1, no. 2, pp. 264–270, 1955.

[63] P. M. Sigmund, "Prediction of molecular diffusion at reservoir conditions. Part 1-measurement and prediction of binary dense gas diffusion coefficients," *Journal of Canadian Petroleum Technology*, vol. 15, pp. 48–57, 1976.

[64] C. K. J. Sun and S. H. Chen, "Tracer diffusion in dense ethanol: a generalized correlation for nonpolar and hydrogen-bonded solvents," *AICHE Journal*, vol. 32, no. 8, pp. 1367–1371, 1986.